 FDMP, vol.6, no.3, pp.291-318, 2010

Electromagnetic DC Pump of Liquid Aluminium: Computer Simulation and Experimental Study

Nedeltcho Kandev[1], Val Kagan[2] and Ahmed Daoud[1]

Abstract: Results are presented of 3D numerical magneto-hydrodynamic (MHD) simulation of electromagnetic DC pump for both laminar and turbulent metal flow under an externally imposed strongly non-uniform magnetic field. Numerous MHD flow cases were simulated using finite element method and the results of five typical examples are summarized here, including one example of laminar brake flow, one example of turbulent brake flow and three examples of turbulent pumping conditions. These simulations of laminar and turbulent channel flow of liquid metal correctly represent the formation of an M shaped velocity profile and are in good agreement with the results of recently published works.
In the case of turbulent flow an interesting effect found in the numerical simulation is the appearance of small current loops located in the zone of decreasing magnetic field.
A prototype of a DC electromagnetic pump for liquid aluminum, using a permanent magnet system, was built and characterized under different operating conditions. Numerous metal flow tests at different electromagnetic force levels were performed successfully. Theoretical and experimental operating characteristics of the pump were also developed. The operating characteristic obtained by numerical modeling is positioned very close to the experimental curve, indicating good agreement between the simulation results and the experimental data.

Keywords: DC magnetic pump, MHD flow, finite element method.

1 Introduction

The concept of electromagnetic pumping (EMP) was created first in the nineteen sixties where it was used in the nuclear industry to pump sodium without any mechanical contact. The EM pump for zinc and later for aluminum was developed in the nineteen seventies.

[1] Institut de recherche d'Hydro-Québec (LTE) Québec, Canada
[2] Hazelett Strip-Casting Corp. Vermont, USA

Today, different EM pump systems are widely used in many liquid metal environments such as extrusion billet casting, metal refinery for transporting molten metals, alloys production etc.

These pumps have been designed without any moving parts and have many advantages over the mechanical pumps including precise flow control, reduced energy consumption and less dross formation. Two different concepts of electromagnetic pumps for molten metals have been developed over the last forty years: a) direct current (DC) electromagnetic pump and b) linear induction electromagnetic (AC) pump.

In a typical direct current (DC) electromagnetic pump, a channel flow of an electrically conducting fluid is submitted to a permanent magnetic field orthogonally oriented to that flow. A direct electrical current is applied across the fluid at a right angle to the flow and at a right angle to the magnetic field, thus producing an electromagnetic Lorentz force which drives the fluid through the channel.

Common problems with both AC and DC pumps are the non-homogeneous distribution of the fluid velocity profile and instability of the flow under certain operation conditions.

Many theoretical investigations of the MHD channel flows and simulation results have been published over the last two decades. Ramos and Winowich (1990) applied finite element method to simulate a magneto-hydrodynamic (MHD) channel flow fields as a function of the Reynolds number, electrode length and the wall conductivity. It is shown that the axial velocity profile is distorted into M – shapes by the applied electromagnetic field and that the distortion increases as the Reynolds number and the electrode length are increased.

In 1993 Lielausis developed the idea concerning the flow structure in an inductive MHD pump channels using results of one dimensional flow model analysis already published by several other researchers in the nineteen eighties.

Hughes, Pericleous and Cross(1995) used two-dimensional models under externally imposed permanent magnetic fields to simulate a laminar MHD flow in macroscopic scale and later, Cho and Hong (1998) studied several analytical solutions using two-dimensional magnetic field analysis based on an equivalent current sheet model.

These theoretical studies and numerical simulations predicted serious problems linked to the transformation of the velocity profile giving the electromagnetic driving force in the opposite direction to the fluid motion, especially at turbulent flow conditions.

In 1979 Holroyd presented the results of an experimental investigation of the flow of mercury along circular and rectangular non-conducting ducts in a non-uniform

magnetic field at high Hartmann number. In this work, flow velocity, pressure and electric potential are measured by hot-films probes. The authors found that the flow in regions of non-uniform magnetic field is greatly disturbed but not in the dramatic manner predicted.

In a recent experimental investigation, Andreev, Kolesnikov and Thess (2006) liquid metal flow in rectangular duct under inhomogeneous magnetic field was studied using the eutectic alloy GaInSn as the working fluid. In the experiments the Hartmann number was fixed at Ha=400 for the range of Reynolds number Re between 500 and 16000.

In 2007, Votaykov and Zienicke investigated the structure of the three-dimensional laminar velocity field in a rectangular duct, using the same geometry and magnetic field configurations as did Andreev, Kolesnikov and Thess (2006). The authors found that the formation of the M-shaped profile in span-wise direction is represented correctly. In addition, they observed a special swirling flow in the corners of the duct caused by Hartmann layer destruction behind the permanent magnets.

The direct current electromagnetic principle has been used mainly to develop electromagnetic micro-pumps for biomedical and chemical applications for precise control of small volume of fluids in micro-channels (Wang, Chang and Chang(2004), Jang and Lee(2000) and Parada and Zimerman (2007)). Electromagnetic DC pumps are not commonly used in the metallurgical industry. The main challenge with this pump is how to conduct a high DC current through the liquid metal inside the pump body. In many practical cases this causes problems with metal contamination, electrode consumption, increased electrical losses etc.

The majority of interesting MHD investigations has treated mainly laminar channel flow and is not concerned with the DC pumping aspect. However, the question of simulating and testing turbulent MHD metal flow, involving braking and pumping aspects, continues to remain open.

In the present study, numerous MHD flow cases were simulated using 3D finite element method and the results of five typical examples have been summarized, including one example of laminar brake flow, one example of turbulent brake flow and three examples of turbulent pumping conditions. These simulations correctly represent the formation of an M shaped velocity profile and are in good agreement with the results of recently published works.

A prototype of a DC electromagnetic pump for liquid aluminum, using a permanent magnet system, was built and characterized under different operating conditions.

Theoretical and experimental operating characteristics of the pump were also developed at different electromagnetic force levels and compared with the simulation results.

2 Physical principle and numerical model

The physical principal of the DC electromagnetic pump is based on the Lorentz electromagnetic force exerted on charged particles in motion in an electromagnetic field.

The geometry of the MHD model considered in this work is shown schematically in Figure 1. A rectangular flat channel with electrically insulated boundaries is filled with liquid metal. This channel is subjected to an externally imposed transversal non-uniform magnetic field B_z using two magnets on the bottom and top walls. The axial horizontal plane $(x - y)$ of the channel (at $z = 0$) is in the half distance of the magnetic gap.

A pair of electrodes is introduced on the vertical lateral walls of the channel at a right angle to the magnetic field. They supply an external electrostatic field E_e with desired magnitude and direction in the molten metal.

In the case considered in this study, where the model must represent a real pump working at different operating conditions including relatively high metal flow, both the laminar and the turbulent flow models must be applied.

The formulation of the steady state magneto hydrodynamic 3D model has been derived from the Maxwell equations (electromagnetic part) for moving medium coupled with the Navier-Stokes equations (fluid dynamics part) for the laminar flow or with the Reynolds-Averaged Navier-Stokes equations and the standard k-ε turbulence model for the turbulent flow. In both flow models, a Newtonian incompressible fluid was considered.

The governing equations used in the numerical simulation can be summarized as follows:

Electromagnetic model:

$$\nabla \times \left(\frac{\nabla \times \vec{A}}{\mu} \right) = \vec{J} \tag{1}$$

$$\vec{J} = \sigma(-\nabla\phi + \vec{u} \times (\nabla \times \vec{A})) + \vec{J}_e \tag{2}$$

$$\nabla \cdot \vec{J} = 0 \tag{3}$$

Laminar flow model:

$$\rho(\vec{u} \cdot \nabla)\vec{u} - \nabla \cdot \left[\eta \left(\nabla\vec{u} + (\nabla\vec{u})^T \right) \right] = -\nabla P + (\vec{J} \times \vec{B}) \tag{4}$$

$$\nabla \cdot \vec{u} = 0 \tag{5}$$

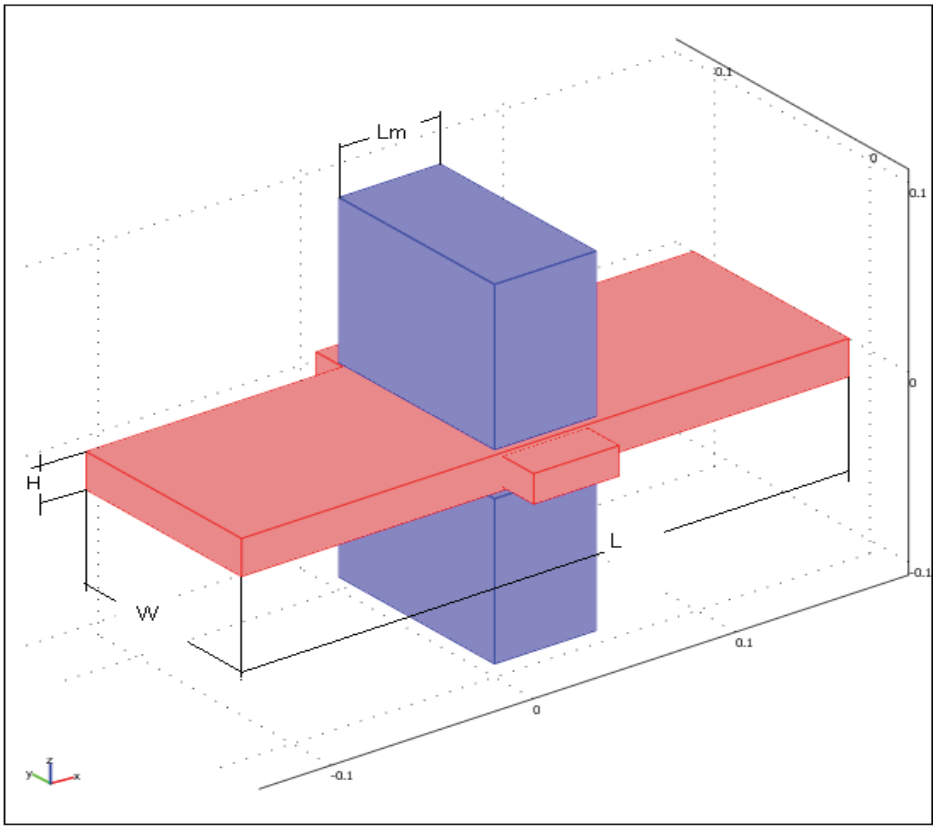

Figure 1: Simplified schema of the MHD model. The channel has length L =0.3 m, height H =0.02 m and width $W = 0.1$ m. The magnet has length Lm = 0.05 m

Turbulent flow model:

$$\rho(\vec{u}\cdot\nabla)\vec{u} - \nabla\cdot\left[(\eta+\eta_T)\left(\nabla\vec{u}+(\nabla\vec{u})^T\right)\right] = -\nabla P + (\vec{J}\times\vec{B}) \tag{6}$$

$$\rho\vec{u}\cdot\nabla k - \nabla\cdot\left[\left(\eta+\frac{\eta_T}{\sigma_k}\right)\nabla k\right] = \frac{1}{2}\eta_T\left(\nabla\vec{u}+(\nabla\vec{u})^T\right)^2 - \rho\varepsilon \tag{7}$$

$$\rho\vec{u}\cdot\nabla\varepsilon - \nabla\cdot\left[\left(\eta+\frac{\eta_T}{\sigma_\varepsilon}\right)\nabla\varepsilon\right] = \frac{1}{2}C_{\varepsilon 1}\frac{\varepsilon}{k}\eta_T\left(\nabla\vec{u}+(\nabla\vec{u})^T\right)^2 - \rho C_{\varepsilon 2}\frac{\varepsilon^2}{k} \tag{8}$$

$$\eta_T = \rho C_\mu \frac{k^2}{\varepsilon} \tag{9}$$

$$\nabla\cdot\vec{u} = 0 \tag{10}$$

The electromagnetic part of the problem is presented by Maxwell-Ampère's law in equation (1), Ohm's law in equation (2) and the conservation of the electrical current in equation (3), where ϕ is the electrical scalar potential,$\vec{A}$ is the magnetic vector potential, $\vec{u}$ is the velocity of the fluid, $\vec{J}$ is the total current density, σ is the electrical conductivity, μ is the permeability and$\vec{J}_e$is the externally generated current density. Here the electrical scalar potential ϕ is determined by solving the Poisson equation: $\nabla^2\phi = \nabla.(\vec{u} \times (\nabla \times \vec{A}))$.

The constants in the equations (1 - 3) are the electrical conductivity σ and the permeability μ. Here the space depended variables are $\vec{A}(x,y,z)$, $\vec{J}(x,y,z)$ and $\phi(x,y,z)$.

Equation (2) can be also formulated equivalently in terms of the electrical field intensity $\vec{E} = -\nabla\phi$, the magnetic flux density $\vec{B} = (\nabla \times \vec{A})$ and externally applied electrical field intensity $\sigma\vec{E}_e = \vec{J}_e$as follows:

$$\vec{J} = \sigma(\vec{E} + \vec{u} \times \vec{B}) + \sigma\vec{E}_e \tag{11}$$

This 3d problem was solved using stationary formulation for the electromagnetic part with induced Lorentz current density term in the moving medium (the current does not move with the moving fluid). This *"quasi-static"* approximation is valid under the assumption that the induced magnetic field is infinitely small in comparison to the externally imposed magnetic field. For the cases considered in this work, where the external field is strong enough (B_0 = 0.46 T with maximum of 0.7 T), this assumption is absolutely acceptable because the numerical simulations and measurements showed that the maximal magnetic field generated by the sum of the induced and externally generated currents is smaller by a factor of about 10^{-5} in comparison to the external magnetic field.

The fluid dynamics part of the problem for the laminar flow model is determined by equations (4) representing the conservation of momentum of the fluid in motion, where P denotes the pressure, ρ is the density and η is the kinematic viscosity of the liquid metal and equation (5) representing the conservation of mass.

The turbulent flow model is determined by equations (6), (7) and (8), representing respectively conservation of momentum, turbulence kinetic energy (k) and dissipation rate (ε) of the fluid. Equation (9) is used to calculate the kinematical turbulent viscosity (η_T) and equation (10) represents the conservation of mass. The constants are: C_μ=0.09, $C_{\varepsilon 1}$=1.44, $C_{\varepsilon 2}$=1.92, σ_k=1 and σ_ε=1.3. In the case of a turbulent flow, two groups of depended variables are chosen: the first group includes the fluid velocity components u (x, y, z) and the pressure P(x, y, z); the second group includes the turbulence components (log(ε) and log(k));

The coupling between the electromagnetic model and the fluid model is achieved by introducing the Lorentz force F, given by the cross product $\vec{J} \times \vec{B}$ as a body force

in the conservation of momentum (equations (4) and (6)) and the use of the fluid velocity calculated by the fluid model in Ohm's law (equation (2)).

The MHD effect depends on the electrical conductivity, the density and the viscosity of the liquid metal. It is characterized by the Hartmann number $H_a = B_0 h\sqrt{\sigma/\mu}$, and by the interaction parameter $N = H_a^2/R_e$. Here R_e is the Reynolds number, given by $R_e = U_0 h/\eta$, $\mu = \rho\eta$ is the dynamic viscosity, U_0 is the mean velocity of the liquid metal and B_0 is the mean magnetic flux density. The Hartmann and the Reynolds numbers are defined here with the half – height of the channel (h=H/2).

3 Numerical modeling of the electromagnetic pump

The problem considered is described in Section II and illustrated schematically in Figure 1.

For this simulation, the liquid aluminum is used as an electrically conductive fluid with density ρ= 2385 kg/m^3, electric conductivity σ= 5e6 S/m and kinematic viscosity ν= 0.545e-6 m^2/s.

The externally imposed non-uniform magnetic field is simulated by introducing two permanent magnets fixed on the top and bottom lateral walls of the rectangular channel and connected to an iron yoke. A DC electrical potential difference can be applied between the two electrodes to impose an external electrostatic field E_e in the molten metal with desired magnitude and direction.

3.1 Boundary conditions

The domain of the flow is given by a rectangular flat channel shown in Figure 1.

For the laminar fluid model, the inlet and outlet boundary conditions of the rectangular channel are determined by the imposed inlet mean velocity U_0 in the x direction and outlet pressure P_{outlet}=0. "No-slip" velocity conditions were considered on the sides, top and bottom walls of the channel.

In the case of turbulent flow, the inlet and outlet fluid boundary conditions are $P = P_{inlet}$ and P_{outlet}=0 respectively. A logarithmic wall function is applied as a boundary condition for the channel walls to represent the turbulent boundary layer.

The electromagnetic domain is delimited by an air sphere. On the external boundaries of this air domain the magnetic and electric conditions are fixed to: $\vec{n} \times \vec{A} = 0$ and $\vec{n}.\vec{J} = 0$, where $\vec{n}$ is normal vector to the boundary. The interior boundaries between the permanent magnets system, the channel and the air assume continuity, corresponding to homogenous Neumann condition. In all simulated cases in this study, electrically insulated boundaries of the channel in the presence of two

electrodes on the vertical walls are considered. The electrical conductivity of the electrode blocks is 3.3e5 S/m.

Coupling of the three different models (magnetostatics, DC conductive media and laminar or k-ε turbulence model) is used to carry out this simulation. The problem is solved using a stationary segregated solver. In one solver iteration, each of the group of variables is solved separately assuming the variables of the other group are constant (values of the last iteration). The problem is considered solved when the residuals of each of the equations previously described are below 1e-3. This method of resolution was chosen because it was more stable than the fully coupled method (only one group of variables).

In this study, 3D numerical simulation based on the finite element method was carried out using the computer package COMSOL Multiphysics 3.4.

Depending upon the case treated, meshing between 75000 and 172000 elements was adopted which generated up to 1 725 000 DOFs. The simulations were run using a Double Quad Xeon 64bits (8 processors) workstation with 8 Gb of RAM. With this computer a simulations where performed in approximately 6 - 8 hours.

4 Simulation results and discussions

The main goal of the numerical investigation is to validate the magneto hydrodynamic hypothesis, and to optimize the pump design considering a highly turbulent metal flow. Different MHD cases are simulated and overall results are summarized below. Two principal applications are simulated: laminar brake flow and turbulent brake or pumping flow at different Lorentz force levels.

4.1 Laminar flow

The first case involves simulating the development of low laminar channel flow at relatively low magnetic field and without any external DC current ($\vec{J}_e = 0$). The goal of this simulation is to validate the MHD brake flow hypothesis at a low Reynolds number and to compare these results with that of other similar published works.

For this case the boundary conditions of the fluid model are determined by the imposed inlet mean velocity U_o = 0.01 m/s and outlet pressure P_{outlet} = 0. As result, the Reynolds number is Re= 183.5, the Hartmann number is Ha = 28.5 and the interaction parameter N = 4.44.

The shape of the externally imposed transversal magnetic flux density $B_z(x)$ along the x axis for z = 0 and y= 0 and the vectors of the velocity field in the central horizontal plane (z = 0) of the studied channel is plotted in Figure 2.

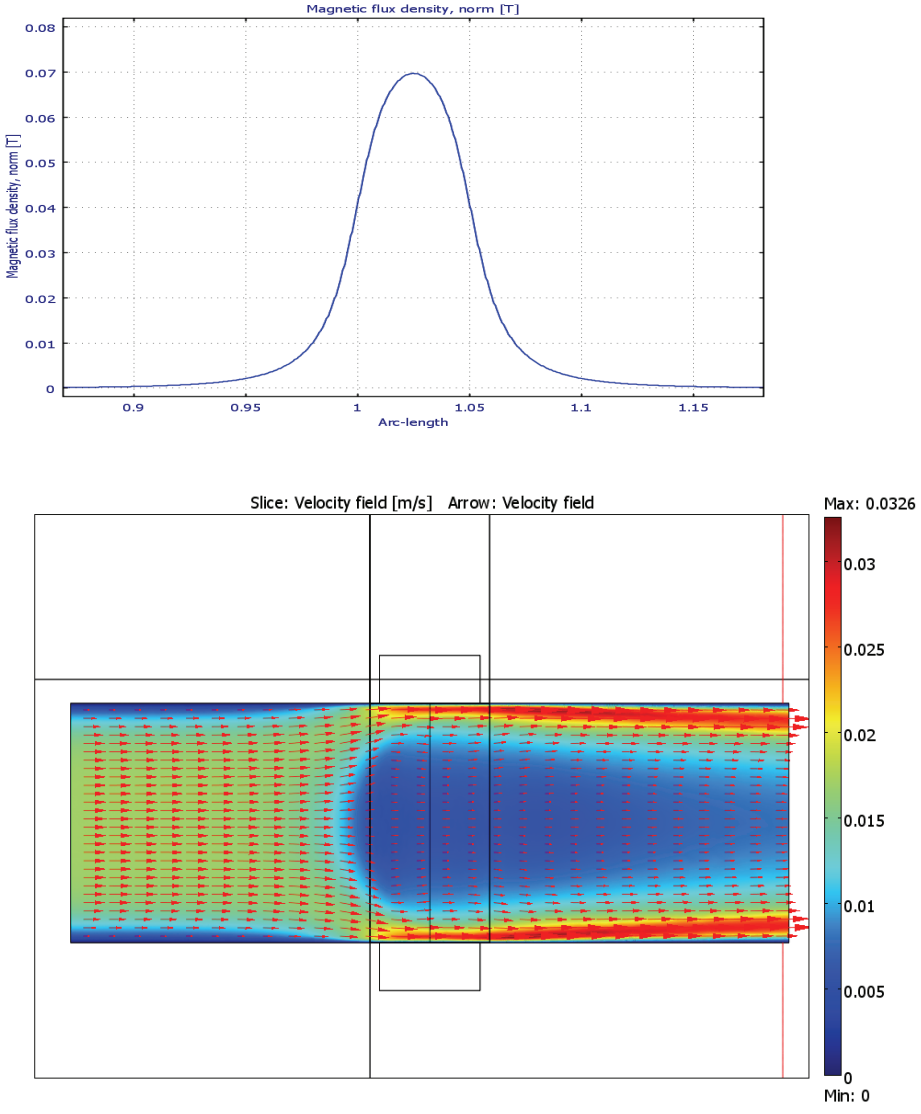

Figure 2: Magnetic flux density $B_z(x)$ along the x axis for $z = 0$ and $y = 0$ (upper part) and the vectors of the velocity field in the central horizontal plane (z = 0) of the studied channel (bottom part)

The maximum magnetic flux density is about 0.07 T and is located in the vertical axis of the magnetic gap.

Notice that all MHD parameters are defined by the overall mean magnetic flux density $B_0 = 0.046$ T

The fluid velocity profile at different fixed positions along the x-axis in the central horizontal plane (z = 0) of the channel $u_x(y)$ is shown in Figure 3.

These two figures show that the originally developed laminar flow profile (see the inlet velocity on Figure 3) undergoes a serious distortion by passing through the magnetic field region. Actually, four typical channel flow regions can be distinguished: a region characterized by constant laminar velocity profile (from the inlet until 1/3 of the channel), a region of flow braking (from the entrance to the exit of the magnetic region), a region of two strong fluid accelerations (near the side walls) and a central part of the channel with very low velocity.

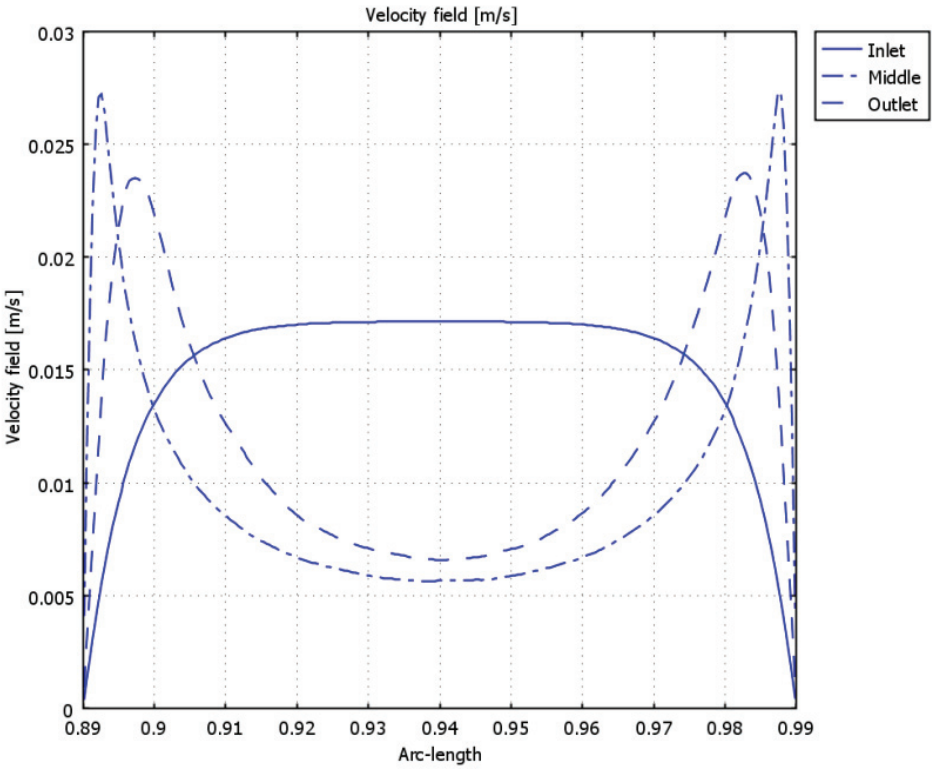

Figure 3: Fluid velocity profile $u_x(y)$ at different positions along the x-axis: Inlet laminar flow (solid curve), middle (dotted curve) and outlet velocity (dashed curve)

This MHD effect can be explained by the fact that the externally imposed vertical magnetic field induces an orthogonal electromotive field in the moving medium producing a current in the negative y direction which flows in closed loop in the liquid metal as illustrated in Figure 4. This current generates a non-uniform negative to the flow electromagnetic Lorentz force $\vec{J} \times \vec{B}$ which counteracts the metal flow in the magnetic zone. This braking force deforms the initially developed laminar or turbulent velocity profile by flatting the velocity boundary layers (Hartmann effect).

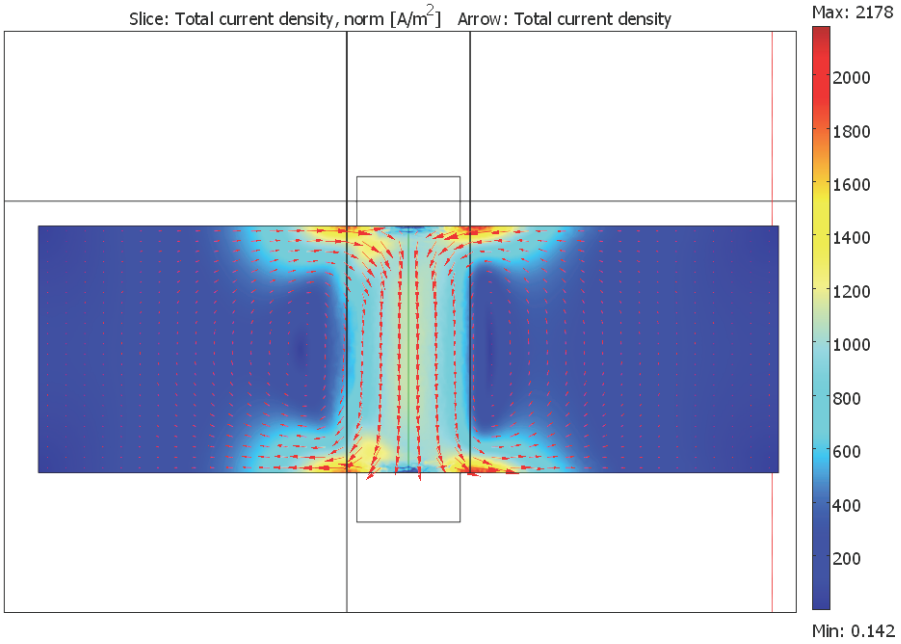

Figure 4: Vector plot of the induced current density in the liquid aluminum in the axial horizontal plane (z = 0) of the channel. *Re*= 183.5, *Ha* = 28.5, *N* = 4.44.

The Lorentz force vector distribution in the axial horizontal plane of the channel is plotted in Figure 5.

The software is able to calculate the elemental Laplace forces dF in each point of the domain and also the total electromagnetic force F acting on the volume of the liquid metal by integrating all forces dF in the 3D domain.

Under the action of this electromagnetic force the inlet laminar velocity profile is disturbed in the magnetic region, developing a typical M shape (see middle and

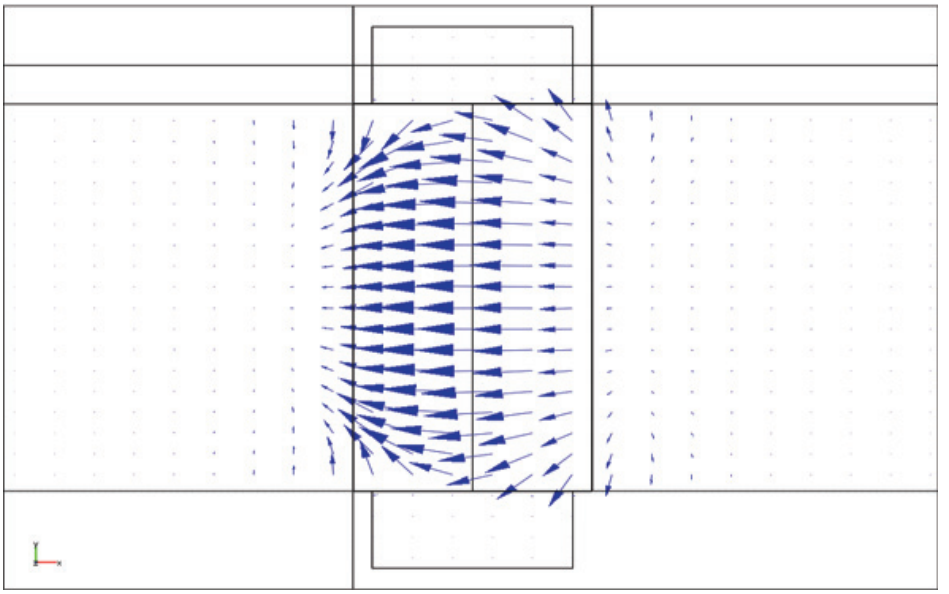

Figure 5: Lorentz braking force vector distribution in the axial horizontal plane (z = 0) of the channel in the magnetic field region. Here the mean value of the force vector in the x direction is -37 N/m^3

outlet velocity profile on Figure 3), which is a demonstration of MHD brake flow process.

These simulation results show that the transformation of the velocity profile under the action of such low magnetic flux density (B_0= 0.046 T) and relatively low Hartmann number (183.5) is, however, significant (U_{max}/U_0=2.7).

Actually, in these conditions the flow is governed mainly by the interaction parameter $N = B_0^2 \sigma h/U_0 \rho$= 4.44 which reflects the ratio between Lorentz and inertial forces.

The simulation of laminar channel flow of liquid metal correctly represents the formation of an M shaped velocity profile and concurs with the results of recently published works.

4.2 Turbulent flow

As mentioned above, in the case considered in this study, a turbulent structure has to be applied where the model simulates a real MHD pump working at high metal flow rate.

This complex MHD problem is not necessarily symmetrical and, therefore, a fully 3D high resolution simulation only will allow seizing all spatial aspects of the flow structure and especially the velocity fields near the channel walls $\boldsymbol{u}(x, y, z)$.

Numerous MHD turbulent flow cases have been simulated and the results of four typical examples are summarized in Tables 1 and 2, including one example of MHD turbulent brake flow and three examples of pumping conditions at different Reynolds numbers and interaction parameters.

The inlet and outlet fluid boundary conditions of this model are $P = P_{inlet}$ and $P_{outlet} = 0$ respectively. The inlet pressure P_{inlet} was considered positive in the case of electromagnetic brake flow simulation and negative in the case of pumping functions. The negative value of the inlet pressure is used to consider a pressure drop in the ducts before the channel.

The remaining fluid boundary conditions are taken as walls with logarithmic function. The external electromagnetic force F_e in Table 2 is determined by the cross product $\vec{J}_e \times \vec{B}$, where J_e is the external DC current, while the electromagnetic force F_{Ltz} is the total Lorentz force acting on the volume of the liquid metal. All forces tabulated in Tables 1 and 2 are referring to the component in the x direction. The forces in the y or z directions are smaller by a factor of 10^{-4} to 10^{-3}.

A parameter $FD{=}Umax/U_0$ was introduced in order to quantify the rate of flow distortion (see Table 2).

The shape of the external transversal magnetic flux density $B_z(y)$ between the two electrodes for $z = 0$ and x = 0 is plotted in Figure 6.

Table 1: Metal flow parameters and simulation results: imposed external potential V_l, imposed inlet pressure P_{inlet}, total external current I_e and total Lorentz force acting on the molten metal F_{Ltz}

Case	**Application**	V_e	P_{inlet}	I_e	F_{Ltz}
		[V]	**[Pa]**	**[A]**	**[N]**
1	Brake flow	0	8800	0	-16.45
2	Pumping	0.24	-13000	1196	28.50
3	Pumping	0.32	-16000	1600	35.92
4	Pumping	0.36	-17000	1794	38.93

Notice that this magnetic field here is about ten times greater (B_0 = 0.46 T with maximum of 0.7 T) than that of the laminar flow case.

The Hartmann number remained the same (Ha = 280) for all four cases because the magnetic flux density was maintained the same, while the Reynolds number varied

Table 2: Results of the simulation: external DC pumping force F_e, mean flow velocity U_0, Reynolds number *Re*, Hartmann number *Ha* and interaction parameter *N*.

Case	F_e	U_0	***Re***	***Ha***	***N***	***Umax/Uo***
	[N]	**[m/s]**				
1	0	0.49	9082	280	8.58	4
2	46.6	0.56	10275	280	7.58	3.8
3	62.1	0.77	14128	280	5.51	3.25
4	69.7	0.88	16110	280	5.05	3.1

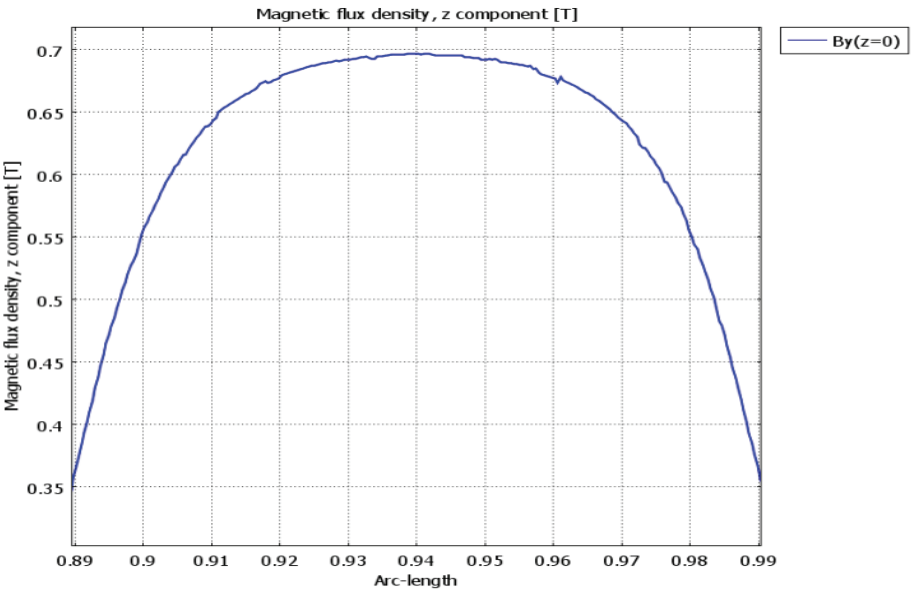

Figure 6: Magnetic flux density, z component $B_z(y)$ along the y axis for $z = 0$ and $x = 0$

from 9082 to 16110, thus changing the interaction parameter*N* between 5.05 and 8.58.

4.2.1 Brake flow

The first case consists of simulating the development of turbulent brake flow at a relatively high magnetic field and without any external DC current ($\vec{J}_e = 0$). The boundary conditions of the fluid model are determined by the imposed inlet con-

stant pressure P_{inlet}= 8800 Pa, outlet pressure P_{outlet} = 0, and a logarithmic velocity function at the walls to represent the turbulent boundary layer. These imposed conditions generated a mean fluid velocity of 0.495 m/s, thus giving Reynolds number *Re*=9082, and interaction parameter N = 8.58.

The shape of the simulated velocity field in the central horizontal plane (z = 0) of the studied channel is plotted in Figure 7.

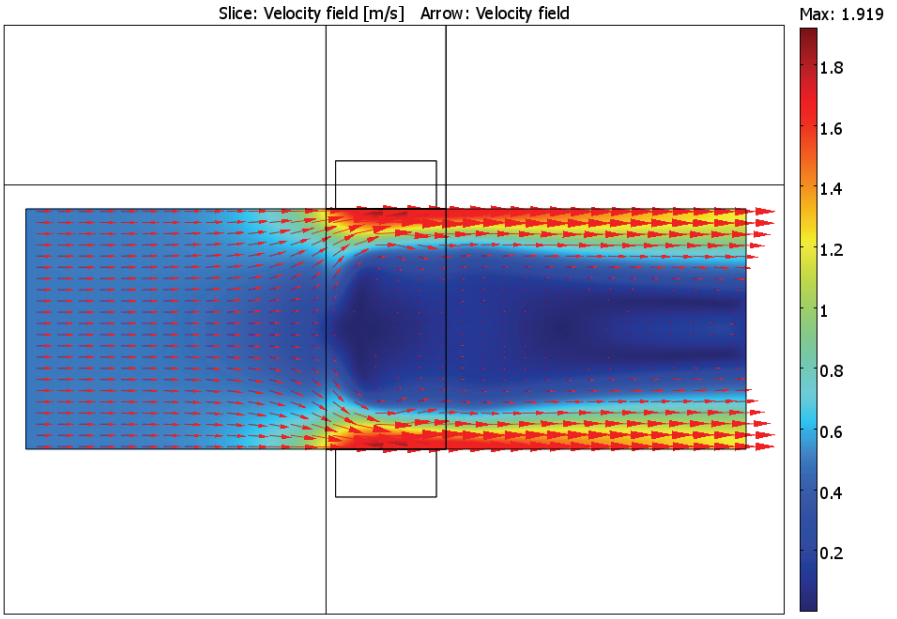

Figure 7: Vectors of the velocity field in the axial horizontal plane (z = 0) of the channel. *Re*=9082, U_0=0.495 m/s.

The fluid velocity profile at different positions along the x-axis in the central horizontal plane $u(y)$ is illustrated in Figure 8.

These results show that the applied magnetic field is strong enough to distort the fluid velocity profile dramatically when the magnetic region is reached.

The maximum to mean velocity ratio in this case is FD = 4, showing a significant transformation of the originally developed turbulent flow profile into M or U chaps (Figure 8).

In the case considered, where the electrical conductivity of the fluid is high, the total braking Lorentz force is sufficiently strong (-16.45 N) and non-uniform to

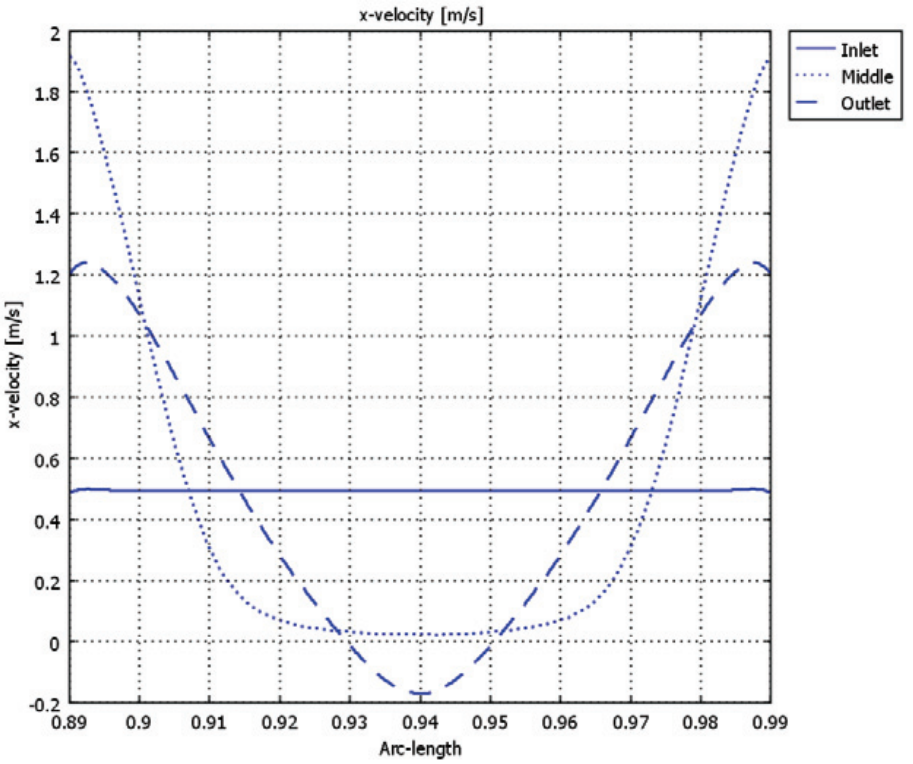

Figure 8: Fluid velocity profile $u(y)$ at different positions along the x-axis: Inlet turbulent flow (solid curve), middle (dotted curve) and outlet velocity (dashed curve)

produce such significant flow destruction causing a high fluid acceleration near the walls and a very low velocity in the central part of the channel.

A negative metal flow arises in the x central part of the channel starting at about 50 mm behind the magnets. The formation of this reverse flow along the center of the channel can be also observed in Figure 9.

This highly non uniform evolution of the flow along the x direction can be explained by the very complicated profile of the electromagnetic braking force determined by the shape of the induced current. It is interesting to observe the distribution of the induced current density vectors showed in Figure 10.

It can be seen that the induced current flows in closed loop in the liquid metal, as

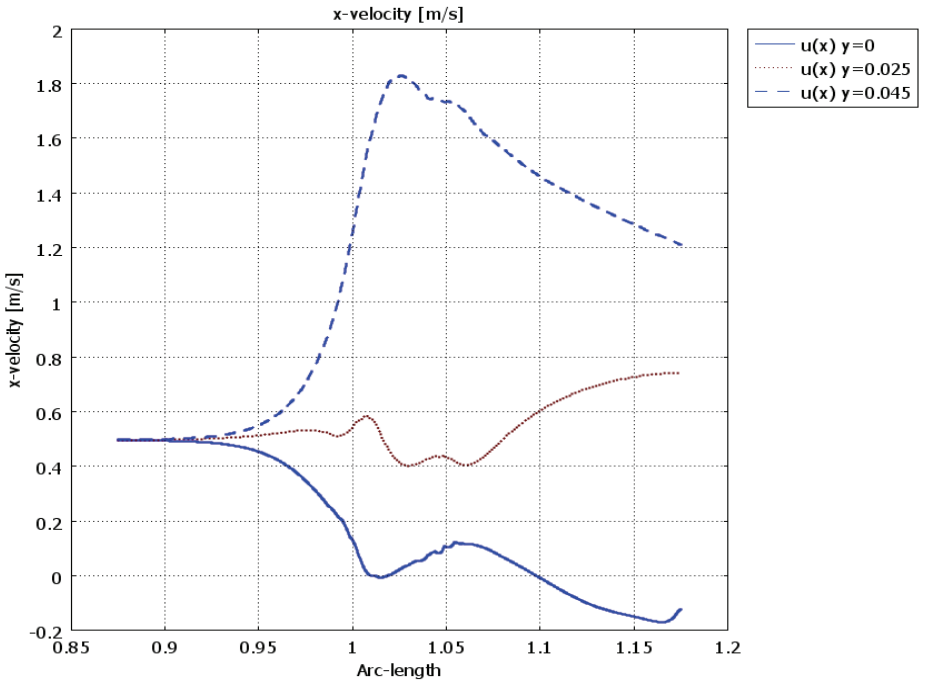

Figure 9: Fluid velocity profile $u(x)$ at three different positions along the y-axis: y=0, 0.025, 0.045 m.

it was found for the laminar flow (see Figure 4). The difference here is that two "strange" current loops arise in the region immediately behind the magnets. The complicated current path is more clearly depicted in the stream line representation of the current shown in Figure 11. These bizarre current "turbulences" are located in the zone of decreasing magnetic field where the electrical field changes its sign.

The competition between the electromotive and the electrostatic components of the electrical field in this area is responsible for this effect and for the perturbation in the velocity profile in the x direction (see Figure 9).

Similar phenomena were observed by Votaykov and Zienicke (2007) for the same channel geometry and magnetic field configuration, despite the fact that their simulations involved laminar flow, while in the case presented here the flow is turbulent.

4.2.2 MHD pump

In static operating conditions (without metal motion), the electromotive field is zero and Ohm's law (Equation 2a) will be reduced to $\vec{J} = \sigma\vec{E}_e = \vec{J}_e$, where $\vec{E}_e$ is

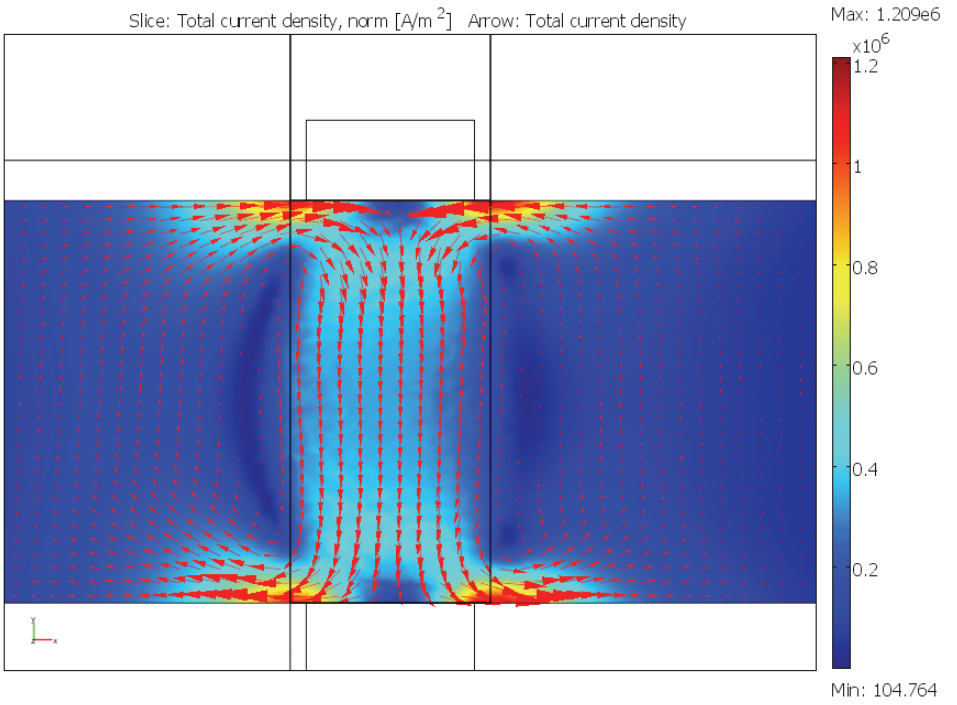

Figure 10: Vectors of induced current density in the liquid aluminum in the axial horizontal plane (z = 0) of the channel

the externally imposed electrostatic field and J_e is the resulting external current. In this case the total electromagnetic force is $\vec{F} = \vec{J_e} \times \vec{B}$ and it is governed by the magnitude of the external electrostatic field and the density of the magnetic field B.

In dynamic pumping operating conditions (with metal flow), the external electrostatic field dominates the induced electromotive field and the resulting current is driven through the liquid metal in the positive y-direction, thus producing electromagnetic force acting in the direction of the flow.

In cases 2, 3 and 4 (see Tables 1 and 2), the imposed electrode potentials are 0.24 V, 0.32 V and 0.36 V, thus generating external currents of 1196 A, 1600 A and 1794 A respectively. The developed external electromagnetic forces are 46.6 N for case 2; 62.1 N for case 3 and 69.7 N for case 4.

The inlet pressures for these three cases are P_{inlet} = -13000 Pa, -16000 Pa and -17000 Pa for case 2, 3 and 4 respectively. These negative pressures have to represent the pressure drops as a function of the flow rate in a real metal transfer circuit. They were determined by calculating the hydrodynamic losses of the experimental

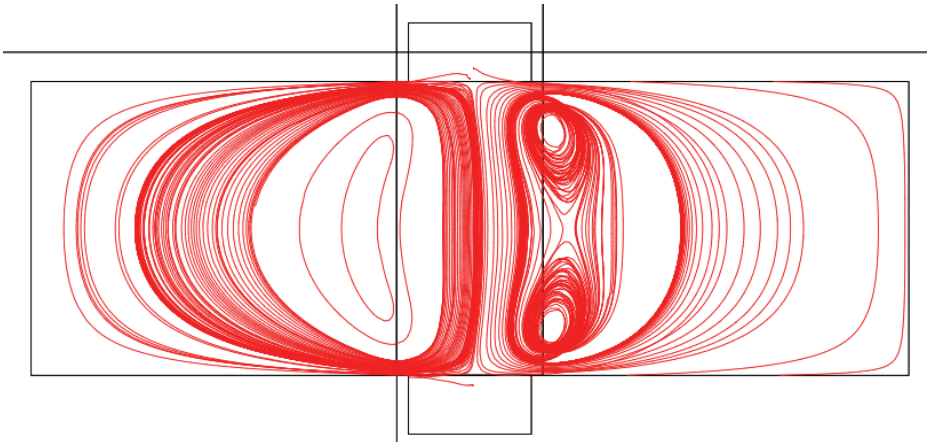

Figure 11: Stream lines of induced current density in the liquid aluminum (Brake flow case 1)

duct used in the test (see equation 11 in §V).

At MHD equilibrium the mean fluid velocities for these three cases are 0.56 m/s, 0.77 m/s and 0.88 m/s respectively. The simulation results show a significant transformation of the originally developed turbulent flow profile into M or U chaps in the magnetic zone for all three cases.

As an example, Figure 12 illustrates the shape of the velocity field in the central horizontal plane (z = 0) of the channel for case 3 and Figure 13 shows the fluid velocity profile at different positions along the x-axis $u_x(y)$ for the same case.

In this case the MHD equilibrium is reached at a mean velocity of 0.77 m/s when the external DC electromagnetic driving forces F_e= 62.1 N compensates completely for the hydrodynamic losses of the fluid transfer circuit and the Lorentz braking force.

Figures 13 shows that the maximum to mean velocity ratio $FD = U_{max}/U_0$ in this case is 3.25, demonstrating a significant distortion of the inlet turbulent flow profile by traveling through the magnetic region.

At a quarter of the distance from the inlet of the channel (0.25L), the velocity profile exhibits relatively low deformation, but it is completely distorted in the next quarter length by entering in the high magnetic field area (see the dashed curve in Figure 13).

The vectors of the induced current density (bottom part) for the case 3 are plotted in Figure 14.

In this case, two new current loops appear in the area before the magnets, thus

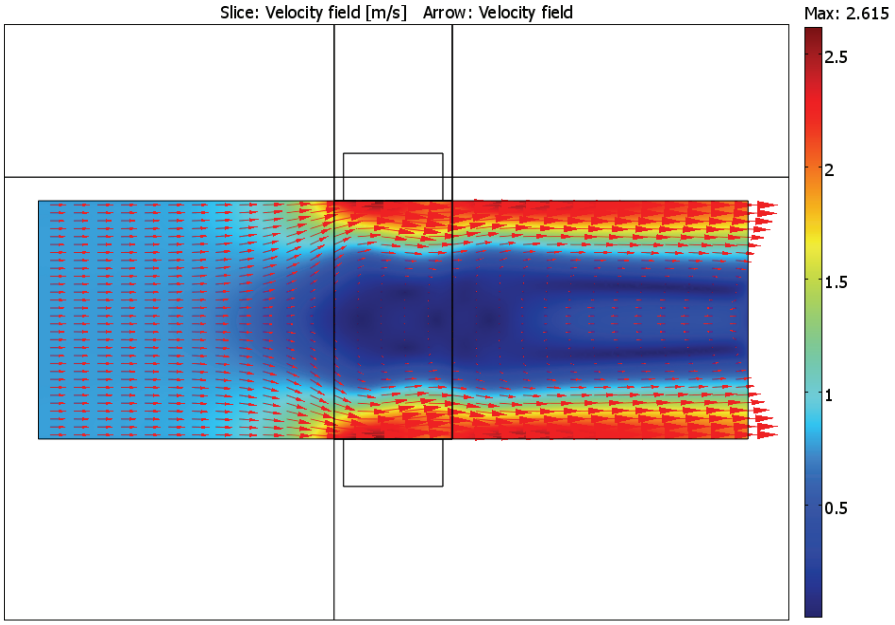

Figure 12: Vectors of the velocity field in the axial horizontal plane (z = 0) of the channel (case 3). Re=14128, N=5.51, U_0= 0.77 m/s.

forming two couples of current turbulences located on both side of the magnetic poles (see Figure 15). The high-resolution 3D numerical simulation made it possible to grasp this complex spatial interaction of electromagnetic and hydrodynamic phenomena at highly turbulent flow.

Figure 16 depicts the vectors of the total Lorentz force density in the axial horizontal plane (z = 0) of the channel. The total electromagnetic force, acting on the volume of the liquid metal, can be obtained by integrating all forces dF in the 3D domain. For this case (3) the total electromagnetic driving force in the $x$direction is 35.92 N.

This figure indicates that the electromagnetic DC driving force is significantly non-uniform and is located in the magnetic region close to the lateral walls.

It can be seen in Table 2 that the parameter $FD=Umax/U_0$ increases systematically with the increase of the interaction parameter. It seems that the distortion of the axial velocity profile into M-shapes is governed mainly by the interaction parameter N for both laminar and turbulent flow and that the degree of this distortion will increase as N increases.

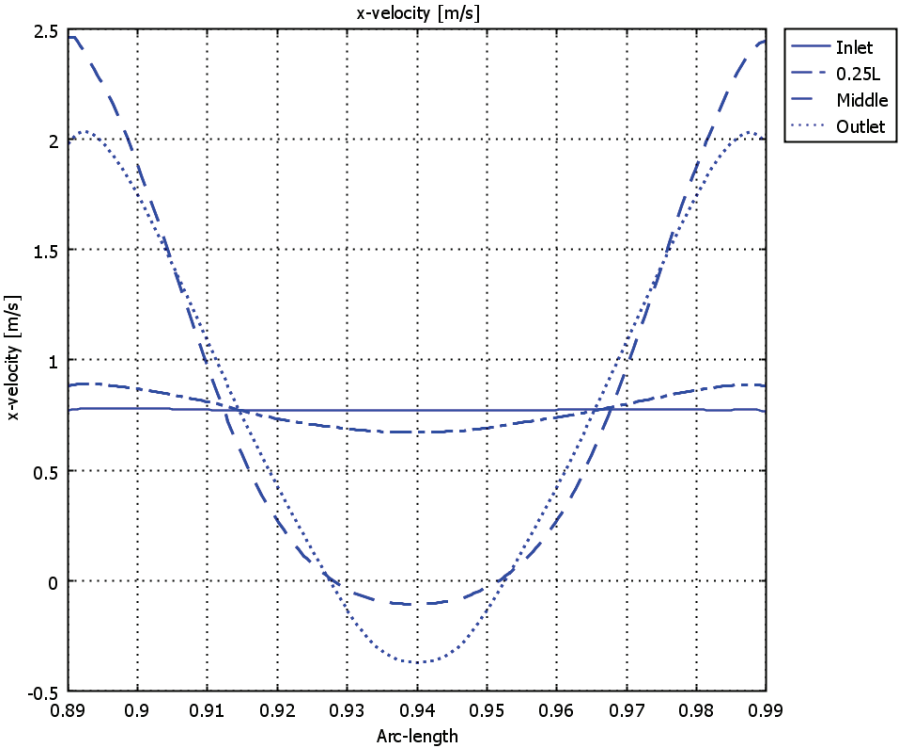

Figure 13: Fluid velocity profile on y-axis $u(y)$ at different positions along the x-axis: Inlet flow (solid curve), 0.25 L from the inlet (dashed dotted curve), Middle (dashed curve) and Outlet velocity (dotted curve)

On the whole, the simulation of laminar and turbulent channel flow of liquid aluminium presented in this study accurately represents the formation of an M shaped velocity profile and corresponds with the results of recently published experimental and theoretical works as Pericleous and Cross (1995), Kolesnikov and Thess (2006) and Votaykov and Zienicke (2007).

5 Pump design and experimental study

A direct current electromagnetic pump was built and tested under different operating conditions. The experiments were conducted using a thermally insulated metallic rectangular channel as pump body, having length L =0.3 m, height H =0.02 m and width W = 0.1m. Liquid aluminum at temperature of about 700˚C, was used as a working fluid with densityρ=2385 kg/m^3, electric conductivityσ=5e6 S/m and

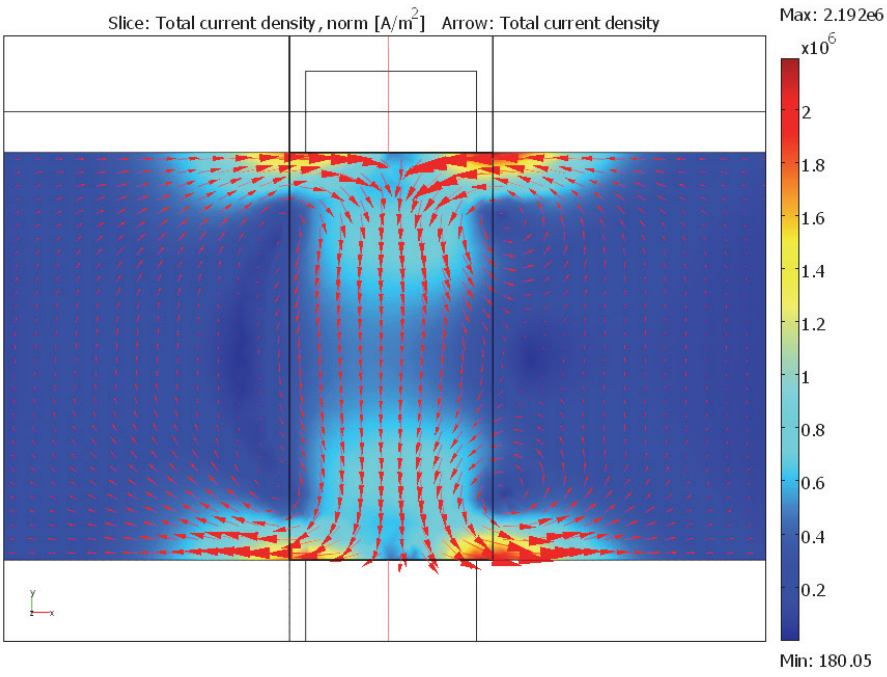

Figure 14: Vector plot of the current density for $z = 0$ and $y = 0$

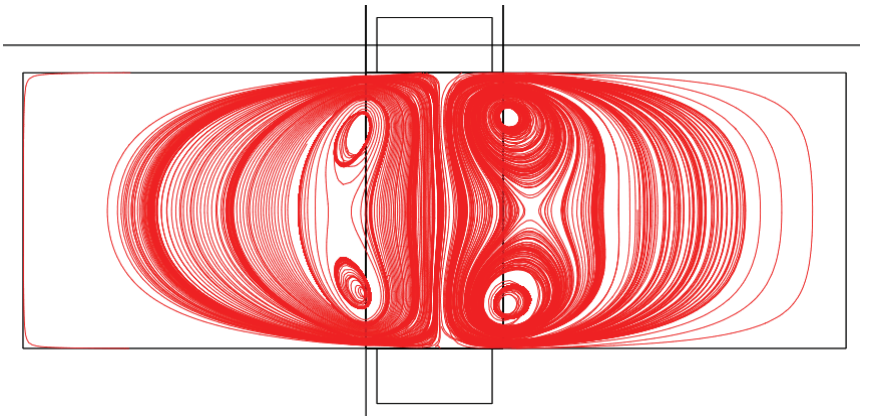

Figure 15: Stream lines of induced current density in the liquid aluminum (Pumping flow case 3)

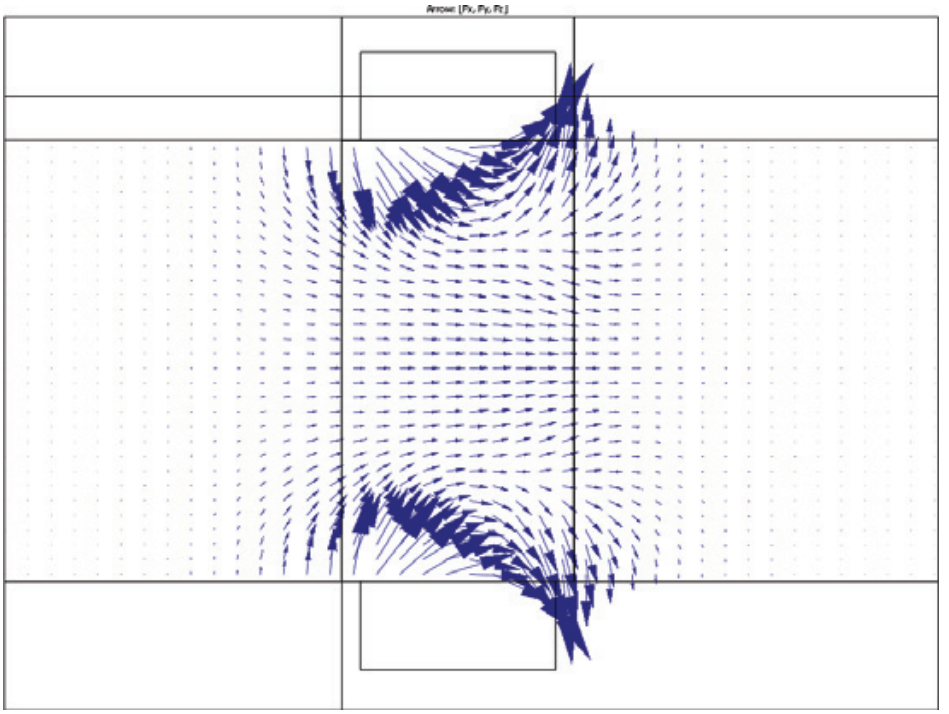

Figure 16: Vector plot of the total Lorentz force F in the axial horizontal plane (z = 0) for case 3

kinematic viscosity ν= 0.545e-6 m^2/s. Remember that these values were used for the computer simulations.

Figure 17 illustrates a simplified schema of the experimental setup including the electromagnetic pump 1 assembled with metal transfer piping system 4 and permanent magnets system 3.

An induction furnace 6 melts the metal to be transferred to the pump body 1 using the tundish 5.

The piping system allows continued circulation of the liquid aluminum in the closed loop circuit (furnace – tundish – EM pump – piping – furnace etc).

The experiments were carried out using a DC electromagnet system or a pair of NdFeB permanent magnets connected to an iron yoke thus forming a magnetic gap of 38 mm. The maximal magnetic flux density in the central point of the gap achieved with this experimental system, was $Bmax$ = 0.78 T

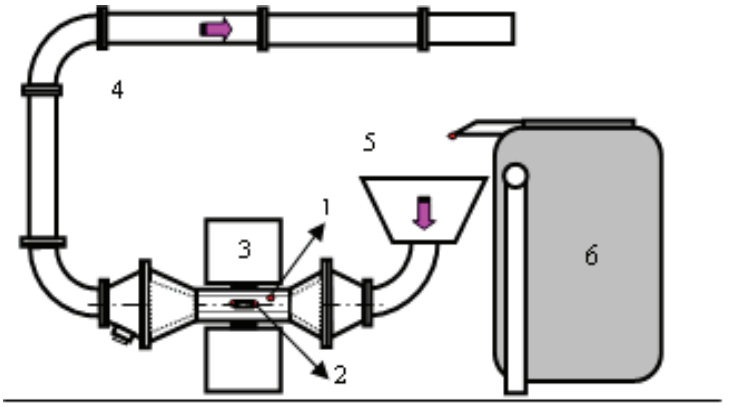

Figure 17: Simplified schema of the test setup including EM pump 1 assembled with permanent magnets 3 and electrodes 2, metal piping system 4, induction furnace 6 and tundish 5

Many dynamic tests were conducted at different operating conditions up to eight hours of continuous circulation of liquid aluminum. Measurements and control of the external DC current, the magnetic field, the temperature at several points and the metal flow were performed continuously during these dynamic tests.

Operating characteristics of the pump were developed at different electromagnetic force levels.

Figure 18 shows an example of theoretical and experimental operating characteristics $U_0(H)$ of the electromagnetic pump.

The evaluation of the hydrodynamic losses of the real metal transfer circuit was used to develop the theoretical operating characteristics.

For the used fluid transfer circuit this function is presented as follows:

$$H = H_{\text{exp}} + k_1 Q^2 + k_2 Q^{1.75} \tag{12}$$

where H_{exp} = 0.5 m is the experimental head and k_1= 1.03E-3 and k_2=6.46E-5 are hydrodynamic constants and Q is the meta flow.

Remember that the negative pressures utilized as inlet boundary conditions in the computer simulations (see §4.2.2) were determined by calculation of the hydrodynamic losses of the experimental duct using equation (10).

The maximum metal head for static conditions (without metal motion) was defined

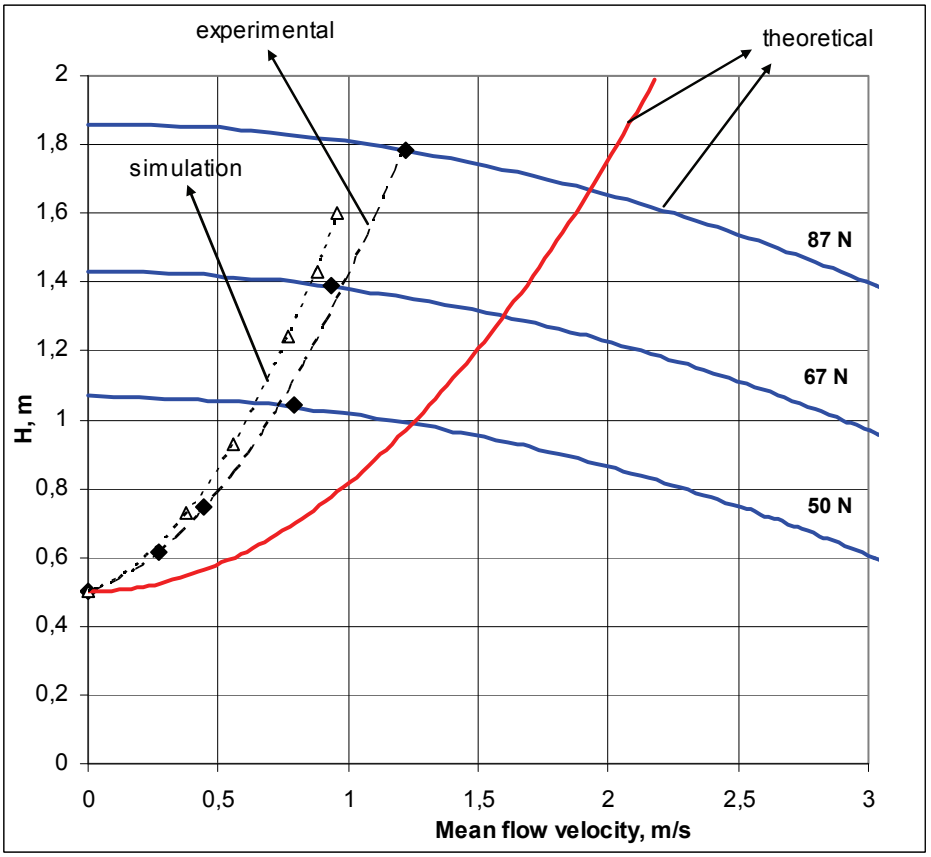

Figure 18: Theoretical (solid curve), experimental (dashed curve) and simulated (triangles curve) operating characteristics of the electromagnetic pump at different external EM force levels F_e

by:

$$H_{\max} = \frac{F_e}{g\rho S} \tag{13}$$

where F_e is the total external electromagnetic force, g is the gravity acceleration constant, ρ is the density of liquid aluminum, S is the cross-section area of the pump body cavity (S=0.002 m^2).

For each test the total external EM force F_e was calculated simply by multiplying the mean value of the measured magnetic field B_o, the external DC current intensity

and the width of the channel W=0.1m:

$$F_e = IB_0W \tag{14}$$

The maximum metal flow at head zero is calculated by using Bernoulli's equation:

$$Q_{\max} = S\sqrt{2\,g\,H_{\max}} \tag{15}$$

where the maximum metal headH_{max} for static condition is determined using equation (11).

The three theoretical curves representing different EM force levels (50, 67 and 87 N) in the operating characteristics were developed using the equation 13 as a function $Q = S\sqrt{2\,g\,(H_{\max} - H)}$ by varying the H from zero toH_{max}.

It should be noted that the theoretical operating characteristic (solid curve) shown in Figure 16 takes into account the hydrodynamic losses of the metal transfer circuit only, while the experimental characteristic (dashed curve) reflects the real consequences of the Hartmann effect. The simulated points (triangles) are located very close to the experimental curve, showing a good agreement between the simulation results and the experimental data. However, the points obtained by simulation (dotted curve) are situated clearly on the left side of the experimental points. This systematic discrepancy between the simulated and experimental points could be explained by certain overestimation of the hydrodynamic losses of the metal transfer piping system calculated by equation (11), and/or by the behavior of the used k-ε turbulence model under the applied MHD pumping flow conditions.

6 Conclusion

Numerical simulations were carried out for liquid metal channel flow. Numerous MHD cases for laminar and turbulent flow were simulated using 3D finite element method. The results of five typical examples are summarized here, including one example of laminar brake flow, one example of turbulent brake flow and three examples of turbulent pumping conditions at different Reynolds numbers and interaction parameter.

For these simulations, the same channel geometry and magnetic field configuration as seen in the experiments of Andreev, Kolesnikov and Thess (2006) and in the computations of Votaykov and Zienicke (2007) were used.

The simulation results of laminar and turbulent channel flow presented in this study correctly portrays the formation of M or U shaped velocity profiles or Hartmann layers at the walls orthogonal to the z component of the magnetic field, and is in good agreement with the results of recently published works.

In the case of highly turbulent flow under pumping conditions, the numerical simulation revealed the appearance of two couples of small current loops located on both side of the magnetic poles. The used fully 3D high resolution simulation allowed seizing this bizarre current "turbulence" effect ensuing from the complex spatial interaction of electromagnetic and hydrodynamic phenomena.

A parameter $FD=Umax/U_0$ was introduced in order to quantify the rate of flow distortion. The results of the simulations showed that this parameter increases systematically with the increase of the interaction parameter. It seems that the distortion of the axial velocity profile into M-shapes is governed mainly by the interaction parameter N for both laminar and turbulent flow and that the degree of this distortion will increase as N increases.

A prototype of direct current electromagnetic pump for liquid aluminum was built and characterized under different operation conditions. Numerous continuous operation tests (up to eight hours) at different current levels and magnetic flux densities were performed successfully. The maximum metal flow rate achieved with this prototype was 25 T/hour (1.4 m/s of mean fluid velocity) at 0.5 m. of metal head.

Operating characteristics of the pump were developed at different electromagnetic force levels and compared with the simulation results. The simulated points are located very close to the experimental curve, showing a relatively good agreement between the simulation results and the experimental data.

References

Andreev O., Kolesnikov Yu., Thess A. (2006): Experimental study of liquid metal channel flow under the influence of a nonuniform magnetic field. *Phys Fluids*, vol 18, 065108.

Gelfag A. Yu, Bar-Yoseph P. Z. (2001): The effect of an external magnetic field on oscillatory instability of convective flows in a rectangular cavity. *Physics of Fluids*, Vol. 13, No. 8, pp. 2269-2278.

Holroyd Richard J. (1979): An experimental study of the effects of wall conductivity, non-uniform magnetic field and variable-area ducts on liquid metal flow at high Hartmann number (Part 1: Ducts with non-conducting walls. *J. Fluid Mech*, vol 93, part 4, pp. 609-630.

Hughes M., Pericleous K. A., Cross M. (1995): The Numerical modelling of DC electromagnetic pump and brake flow. *Appl. Math. Modelling*, Vol. 19, pp. 713-723.

Jang J.; Lee S. S. (2000): Theoretical and experimental study on MHD micropump. *Sens. Actuators A,* Vol. 80, pp. 84-89.

Lielausis O. (1993): Development of ideas concerning the flow structure in inductive MHD pump channels, *Magneto-hydrodynamics,* Vol. 29, No. 4.

Mahmud S., S. H. Tasnimand M. H. Mamun (2003): Thermo-dynamic analysis of mixed convection in a channel with transverse hydro-magnetic effect. *Int. J. of Thermal Sciences*, Vol. 42, pp. 731-740.

Parada Jaime H. L., William B.J. Zimerman (2007): Numerical simulation of a magnetohydrodynamic DC microdevice. *Multiphysics Modelling with Finite element methods*, Vol. 18, pp. 375-391.

Pei-Jen Wang, Chia-Yuan Chang, Ming-Lang Chang (2004): Simulation of two-dimensional fully developed laminar flow for a magneto-hydrodynamic (MHD) pump. *Biocensors and Bioelectronics*, Vol. 20, pp. 115-121.

Ramos I. J., Winowich N. S. (1990): Finite difference and finite element methods for MHD channel flows. *Int. J. Num. Methods*, Vol. 11, pp. 907-934.

Suwon Cho, Sang Hee Hong (1998): The magnetic field and performance calculations for an electromagnetic pump of a liquid metal: *J. Phys. D: Appl. Phys.*, Vol. 31, pp. 2754-2759.

Votaykov Evgeny V., Zienicke E. A. (2007): Numerical study of liquid metal flow in a rectangular duct under the influence of a heterogeneous magnetic field. *FDMP: Fluid Dynamics & Materials Processing*, Vol. 1, pp. 101- 117.